JOURNAL OF PROPULSION AND POWER
Vol. 18, No. 4, July–August 2002

Control of Low-Pressure Turbine Separation Using Vortex-Generator Jets

Rolf Sondergaard* and Richard B. Rivir†
U.S. Air Force Research Laboratory, Wright–Patterson Air Force Base, Ohio 45433-7251
and
Jeffrey P. Bons‡
Air Force Institute of Technology, Wright–Patterson Air Force Base, Ohio 43433-7765

The application of vortex-generator jets to control separation on the suction surface of a low-pressure turbine blade is reported. Blade Reynolds numbers in the experimental, linear turbine cascade match those for high-altitude operation of many aircraft gas-turbine engines, as well as the last stages of industrial ground-based gas turbines. Results are presented for steady blowing at jet blowing ratios from zero to four and at several chordwise positions and two freestream turbulence levels. Findings show that above a minimum blowing ratio, which is dependant on the injection location, the pressure loss in the modified blade's wake is reduced by a factor of between two and three. Boundary-layer traverses show that separation is almost completely eliminated with the application of blowing. No significant deleterious effects of vortex-generator jets are observed at higher (nonseparating) Reynolds numbers. The addition of 4% freestream turbulence to the cascade freestream lowers the separation Reynolds number of the turbine blade studied, but does not eliminate the effectiveness of the control technique. The vortex-generator jet control strategy is demonstrated to be a viable technique for low-pressure turbine separation control.

Nomenclature

B	=	jet blowing ratio, $(\rho u)_{\text{jet}}/(\rho u)_{\text{loc}}$
C_x	=	axial chord length, 17.8 cm
c_d	=	jet hole discharge coefficient
c_p	=	blade pressure coefficient $(p_{t,i} - p_{\text{loc}})/q_i$
d	=	jet hole diameter, 1 mm
L	=	blade loading parameter [see Eq. (1)]
l	=	jet hole length, 8 mm
p	=	pressure, Pa
q	=	dynamic pressure, $\rho u^2/2$, Pa
Re	=	inlet Reynolds number, $\rho_i u_i C_x/\mu$
T_u	=	freestream turbulence in percent
u	=	streamwise mean velocity, m/s
u'	=	streamwise rms fluctuating velocity, m/s
γ	=	blade pressure loss coefficient, $(p_{t,i} - \bar{p}_{t,o})/q_i$
γ_{loc}	=	local blade pressure loss coefficient, $(p_{t,i} - p_{t,\text{loc}})/q_i$
μ	=	dynamic viscosity, kg/m s
ρ	=	density, kg/m^3

Subscripts

i	=	cascade inlet conditions, reference
jet	=	vortex-generator jet conditions
loc	=	local blade midchannel conditions
o	=	cascade outlet conditions
t	=	stagnation or total conditions

Superscript

$\bar{}$	=	pitch-averaged quantity

Received 16 June 2000; revision received 5 October 2001; accepted for publication 7 October 2001.

*Engineer, Turbine Branch, Turbine Engine Division, Propulsion Directorate Building 18, 1950 Fifth Street. Member AIAA.
†Engineer, Turbine Branch, Turbine Engine Division, Propulsion Directorate Building 18, 1950 Fifth Street. Fellow AIAA.
‡Associate Professor, Department of Aeronautics and Astronautics, Building 640, 2950 P Street. Member AIAA.

Introduction

DURING high-altitude cruise, the operating Reynolds number (based on axial chord and inlet velocity) for the low-pressure turbine (LPT) in an aircraft gas-turbine engine can drop well below 2.5×10^4. This low Reynolds number condition is particularly acute in the class of small gas-turbine engines typically used or planned for use in many high-altitude uninhabited air vehicles. At these low Reynolds numbers, the boundary layers on the LPT blades are largely laminar, even in the presence of high freestream turbulence. This makes the blades very susceptible to flow separation near the aft portion of the blade suction surface. Such separation causes a significant increase in losses through the turbine stage, with an associated system-level performance drop. Sharma[1] showed a nearly 300% increase in loss coefficient at Reynolds numbers below 9.5×10^4 compared to the loss coefficient at higher Reynolds numbers for the particular geometry he examined. This increase was found to be primarily due to separation occurring over the trailing 50% of the suction surface. This increased loss translates to a significant decrease in both turbine efficiency and loading at these operating conditions. Altering the blade shape to avoid this low Reynolds number separation problem is not usually practical because such a modification is likely to impair the engine operation at higher design (usually takeoff) Reynolds numbers. As such, separation control strategies are of interest.

Boundary-layer separation control in diffusing flows (under pressure conditions similar to the aft portion of a turbine blade) has been studied in the laboratory for many years. Lin et al.[2] presented results from a number of passive and active strategies employed with varying degrees of success in a backward-facing, curved-ramp wind-tunnel facility. Strategies investigated included submerged vortex-generators, large-eddy breakup devices, elongated boundary-layer arches, flush-mounted Helmholtz resonators, and vortex-generator jets (VGJs). Of those studied, only the last two, Helmholtz resonators and VGJs, are active techniques. Active techniques have the advantage that they can be shut off when not required for flow control. This is especially desirable for turbine blade application because any passive control strategy that is successful at low Reynolds number boundary-layer control could increase the blade's drag penalty and/or surface thermal loading at higher Reynolds numbers where the control is not required. Of the active strategies examined by Lin et al., only VGJs had a significant effect on reducing

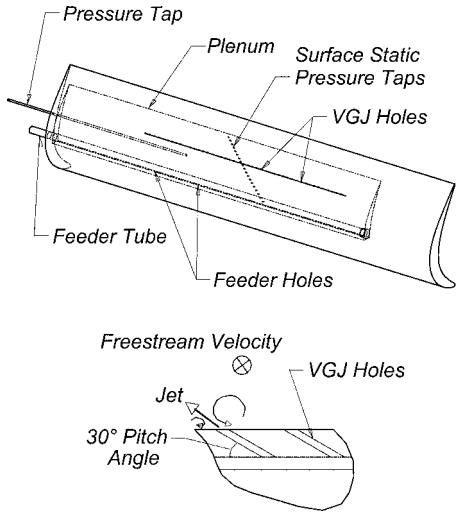

Fig. 1 ASC blade and blade cross section detail showing hole geometry.

diffuser separation. VGJs were also studied extensively in separation control experiments on flat plates under adverse pressure gradients by Johnston and Nishi[3] and Compton and Johnston.[4] Their work shows VGJs are particularly well suited for boundary-layer separation control.

VGJs are typically configured with a low pitch angle (30–45 deg) and aggressive skew angle (45–90 deg) to the local freestream flow direction. Here, pitch angle is defined as the angle the jet makes with the local surface, and skew angle is defined as the angle of the projection of the jet onto the surface relative to the local freestream direction. In this skew configuration, the VGJ creates a horseshoe vortex pair with one very strong leg accompanied by a weak leg of opposite sign, as shown in Fig. 1. The result is a single, dominant, slowly decaying streamwise vortex downstream, rather than the two weaker counter-rotating horseshoe vortices generated by a jet with 0-deg skew or a symmetric passive boundary-layer obstruction. It has been shown[3] that this single-sign vortex energizes the separating boundary layer by effectively bringing high-momentum freestream fluid down to the wall. This experimentally based explanation for the effectiveness of VGJs has more recently been corroborated by a numerical calculation performed by Henry and Pearcey.[5] Their work shows clearly the development of a single, dominant vortex for a VGJ at high skew angles (vs the two-vortex structure at 0-deg skew). Their predictions of the VGJs' beneficial effects are validated against the Compton and Johnston[4] data. The success of this control strategy has been demonstrated with both laminar and turbulent boundary layers,[6] though the vortex structure is subtly different in the two cases.

These reports documenting the favorable results related to the use of VGJs for boundary-layer separation control have led to the present investigation into turbine separation control at low Reynolds numbers. Of the various passive and active control options, VGJs are attractive due to the ability to shut them off when desired, thus eliminating the risk of negative effects during high Reynolds number turbine operation. Also, though LPT blades are traditionally uncooled (though some modern high-performance engines now have cooled LPT stages), engine manufacturers have years of proven experience fabricating high-pressure turbine (HPT) blades with film cooling holes that have essentially the same physical dimensions and flow rates as VGJs. Bleed air from an engine compressor stage could be made available to these LPT VGJs in the same way that it is currently routed to the HPT cooling passages. The thermodynamic cycle costs of implementing VGJs on the LPT are likely to be insignificant compared to those already incurred by implementing film cooling on the HPT. This is because the mass flow rate required is relatively insignificant, and bleed air could be drawn from the low-pressure compressor. Complexity and weight issues would have to be addressed for a practical application, of course. Given these considerations, an experimental study of active separation control using jet- (VGJ-) induced boundary-layer vortices was conducted in a low-speed linear cascade using a prototypical LPT blade profile. This report documents the success of this implementation using steady forcing at several chordwise stations in the separated zone of the blade suction surface. The effects of jet blowing ratio, jet location, operating Reynolds number, and freestream turbulence are also presented.

Experimental Facility

An induction wind tunnel housed the linear turbine cascade used in this study. A 125-hp electric motor powers an axial flow fan, drawing air at inlet velocities up to 80 m/s through an 0.85 m tall by 1.22 m wide test section. This translates to a maximum Reynolds number of approximately 1×10^6 based on the axial chord of the current blade. Inlet velocity and axial chord were chosen as reference quantities because they are both easily measurable. To convert to a Reynolds number based on true chord, multiply by 1.1. To convert to Reynolds number based on suction side length, multiply by 1.46. To convert to Reynolds number based on design exit velocity, multiply by 1.64.

The entrance to the tunnel consists of a 3.0×2.7 m rectangular bell-mouth inlet. Honeycomb flow straighteners located in the inlet, combined with a gradual 8:1 area contraction, produce a uniform, low-turbulence velocity profile at the cascade test-section inlet. Flow velocity uniformity is within $\pm 1\%$ at a Reynolds number of 1×10^5 with less than 1% freestream turbulence measured 0.64 axial chord lengths C_x upstream of the cascade. This background level of turbulence can be augmented to more nearly match that of the flowfield in an operating turbine engine through the use of a turbulence generating grid located approximately $10C_x$ upstream of the cascade. The turbulence grid consists of a square-mesh array of 2.54-cm- (1-in.) diam tubes spaced 7.6 cm (3 in.) apart and produces freestream turbulence levels of approximately 4% at the $0.64C_x$ upstream station. The uniformity of turbulence across the cascade is $\pm 0.3\%$ with an integral length scale of approximately 2.5 cm (1 in.).

The linear cascade consists of eight 0.88-m (34.5-in.) span, 0.18-m (7-in.) axial chord C_x blades, plus two partial blade endwalls. The blades were fabricated from molded polyurethane and are affixed to the test section using bolted end mounts. The two-dimensional blade shape studied is the Pratt and Whitney PakB research design, which is a low Mach number scaled version of a modern highly loaded LPT blade design. The cascade has a solidity (axial chord to blade spacing) of 1.13, an inlet flow angle of 55 deg, and a design exit angle of 30 deg (both angles measured from the plane of the cascade). The innermost and outermost two blades (1, 2, 7, and 8) are close to the cascade exit tailboards and, thus, are unsuitable as test blades. Blades 4 and 6 are each instrumented in the center 0.2 m of their span around both pressure and suction surfaces with 40 1-mm-diam static pressure taps for measurement of full blade pressure coefficient c_p profiles. Blade 5 is instrumented with 19 pressure taps on the suction side of the blade between 47 and 89% axial chord spaced every 6.4 mm (0.25 in.). Tygon tubes from the pressure taps on all three blades are fed through the blade cores to a selector valve and then to a 250-Pa (1.0-inch water) full-scale pressure transducer that references to an upstream total pressure probe. Uncertainties in the pressure measurement translate to an uncertainty of approximately ± 0.05 in c_p and ± 0.02 in γ at $Re = 2.5 \times 10^4$.

The active separation control (ASC) blade mounted in position 5 of the cascade was manufactured with a hollow cavity running the span of the blade and covering the region from 40 to 90% axial chord (Fig. 1). Fittings at the lower end of the blade allow for feed air for the VGJs and cavity static pressure measurement. A needle-valve located upstream of the feed port allows fine control of the mass flow rate into the blade cavity. Air exhausts from this valve into a 1.2-cm- (0.5-in.-) diam capped copper tube running the span of the cavity. There are 25, 1.5-mm- (0.06-in.-) diam holes spaced every 2.54 cm (1 in.) along the copper tube that produce a spanwise uniform supply of air to the VGJs. The 1-mm- (0.04-in.-) diam d cylindrical VGJ holes were drilled from the exterior surface of the blade, through the approximately 4-mm (0.16-in.) thick wall, and into the cavity with a 30-deg pitch angle and a 90-deg skew angle. The VGJ holes

have an aspect ratio (l/d) of approximately 8 and are spaced every $10d$ along the center 0.46 m (18 in.) of the ASC blade span. For this study, rows of VGJs were placed at 45, 53, 63, 73, and 83% C_x. Each row was studied independently, with the unused rows covered by a piece of 0.05-mm-thick tape (sufficiently thin to avoid tripping the boundary layer). Flow separation nominally occurs around 70% C_x on the baseline, uncontrolled blade when operated at a Reynolds number of 4.5×10^4 or below. The discharge coefficient c_d of the holes was measured to be 0.6 ± 0.03, and flow velocity variation among the 45 VGJ holes in each row was verified to be less than $\pm 5\%$. When the tunnel was in operation, the cavity pressure was monitored using a pressure transducer with an accuracy of ± 5 Pa. This measurement, along with the VGJ hole discharge coefficient, allowed for an estimation of the jet centerline velocity to within $\pm 10\%$. The jet blowing ratio B was computed as the ratio of the jet exit velocity to the local freestream velocity as calculated from the local pressure coefficient.

Fixed upstream flow instrumentation consists of thermocouples for inlet temperature measurement and an upstream pitot-static reference probe. Four 1.5-m- (60-in.-) long transverse slots are located along the top of the cascade section at 0.64 and $1.22C_x$, both upstream and downstream of the cascade cassette. Probes mounted on a three-axis traverse located atop the tunnel facility can be used to map a planar cross section of the wind tunnel through any of these four slots. All downstream traverse data presented in this paper were taken using slot 3, located $0.64C_x$ downstream of the blade trailing edges, with the probe sensor at midspan. Loss coefficients were measured using a Kiel probe with a 1.5-mm- (0.06-in.-) diam sensor head plumbed to the 250-Pa (1.0-inch water) transducer. Errors on the loss coefficient are on the order of $\pm 5\%$ at a Reynolds number of 1×10^5 and $\pm 10\%$ at a Reynolds number of 2.5×10^4. All velocity profiles were measured using a single 4-μm-diam tungsten hot wire. Each velocity measurement consists of a minimum of 40,000 individual data samples taken at a 10-kHz sample rate. This sample rate was deemed adequate to capture the relevant flow frequencies at the velocities studied (<1 kHz). The mean u and rms fluctuating u' velocities were calculated from the raw data. The velocity computation algorithm corrects for variations in ambient pressure, temperature, and humidity.

A microtraverse system, mounted inside the test section, was used to make boundary-layer profile measurements at several chordwise locations on the ASC blade. This microtraverse, with 5 cm of total travel, is controllable in steps of less than 2 μm. It was located outside the outer tailboard and accessed the ASC blade through a longitudinal slot in the tailboard. A single 25-μm by 0.25-mm subminiature hot-film probe was mounted on the microtraverse.

When compared to a collocated pitot-static probe velocity measurement, the error in the hot wire and film probes was within $\pm 2\%$ at flow rates of interest. The three-axis traverse position is accurate to within ± 0.5 mm and the microtraverse position is accurate to within ± 0.01 mm.

Results and Discussion

To demonstrate properly the usefulness of vortex-generator jets for boundary-layer separation control, the flow separation must be documented for the uncontrolled case before proceeding with the results of the controlled cases. This section will present first the baseline performance without blowing, followed by the results with blowing. The effects of blowing ratio, blowing location, flow Reynolds number, and freestream turbulence will then be examined in detail.

Baseline Case ($B = 0$)

Figure 2 shows a survey of γ vs Reynolds number based on inlet velocity and axial chord for the baseline case. The data are taken behind blade 5, the center blade of the cascade. The pressure loss coefficient is a direct measure of the irreversible losses associated with the blade aerodynamics. Note that this is an area-averaged quantity rather than a mass-averaged one as is often presented. This was necessary because simultaneous total pressure and velocity data were unavailable. The difference between the two definitions for this

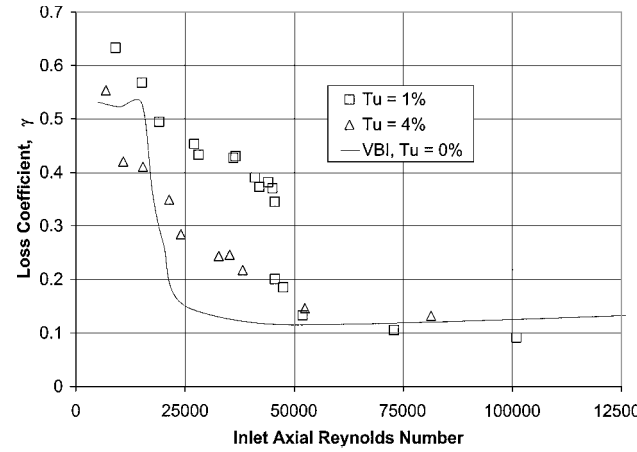

Fig. 2 Loss coefficient γ vs inlet Reynolds number: $T_u = 1\%$, $T_u = 4\%$, and VBI prediction ($T_u = 0\%$).

application is approximately 5% and, therefore, not considered significant because changes in loss level are of primary interest here. Also shown in Fig. 2 is a Reynolds-averaged Navier–Stokes computational fluid dynamics calculation using the two-dimensional vane blade interaction (VBI) code.[7] VBI is an unsteady Reynolds-averaged Navier–Stokes code employing the algebraic Baldwin–Lomax boundary-layer turbulence model, which does not account for freestream turbulence. The code was run in single row, steady flow mode for the calculation. There is a sudden significant increase in aerodynamic losses for the low inlet turbulence (1%) case for inlet Reynolds numbers below 5×10^4. This increase in loss is due to an abrupt onset of separated flow, which, in the presence of low freestream turbulence, remains separated for the full length of the blade. In the presence of higher inlet turbulence (4%) the increase in loss begins at roughly the same Reynolds number, but the rise in losses is more gradual. This is because the higher freestream turbulence causes the boundary layer to be transitional at lower Reynolds numbers and, therefore, less susceptible to separation. Thus, separation is delayed at higher turbulence levels; it begins farther back on the suction surface at higher turbulence levels. In addition, once separation does occur, increased freestream turbulence causes the shear layer above the separation bubble to transition, allowing it to reattach before the end of the blade. At an inlet Reynolds number of 2.5×10^4, the loss coefficient has increased by a factor of four for the low-turbulence case and a factor of two and a half for the higher-turbulence case. Because an inlet Reynolds number of 2.5×10^4 is well within the range of operating Reynolds numbers of engine systems, this was chosen as the baseline Reynolds number for testing.

The baseline, unblown blade surface c_p profile is shown in Fig. 3 for inlet Reynolds numbers of 2.5×10^4, 4.2×10^4 and 8.5×10^4 with low (1%) freestream turbulence. The data shown are from blade 6 (adjacent to the primary test blade). The plateau in each dataset on the back half of the blade on the suction surface, where the c_p data depart from the calculated profile, is associated with the regions of boundary-layer separation. At a Reynolds numbers of 2.5×10^4 and 4.2×10^4, the flow separates near 70% C_x, which roughly corresponds to the beginning of uncovered turning on this blade profile, and remains separated past the trailing edge. At a Reynolds number of 8.5×10^4, the separation point has moved back somewhat to approximately 75% C_x, and the bubble has shrunk significantly, reattaching by approximately 85% C_x. The VBI calculations show a similar trend, with the Reynolds number 2.0×10^4 case showing a separation near 70% C_x and the Reynolds number 1×10^5 showing essentially attached flow. As Fig. 3 shows, the extent of this region increases with decreasing Reynolds number, which is in agreement with the measured increase in loss coefficient discussed earlier.

Figure 4 shows the local loss coefficient γ_{loc} behind blade 5 over a similar range of Reynolds numbers. As the Reynolds number drops and the flow separates on the suction side, the wakes grow much wider with a greater peak total pressure loss. The wakes also shift

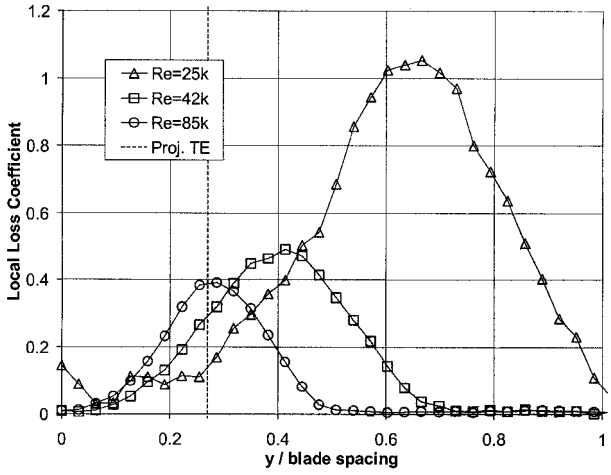

Fig. 3 Surface pressure coefficient vs axial chord for baseline blade: experimental data for $Re = 2.5 \times 10^4$, 4.2×10^4, and 8.5×10^4 with $T_u = 1\%$ and VBI predictions for $Re = 2.0 \times 10^4$ (fully separated flow) and $Re = 1.0 \times 10^5$ (small separation bubble with reattachment), $T_u = 0\%$.

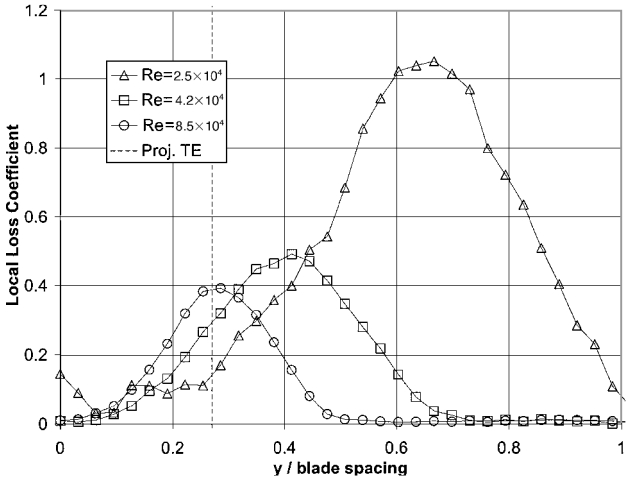

Fig. 4 Local pressure loss coefficient γ_{loc}; traverses across exit wakes at 0.62 axial chords downstream from blade trailing vertical dashed line is trailing-edge projection based on inviscid flow: $Re = 2.5 \times 10^4$, 4.2×10^4, and 8.5×10^4, $T_u = 1\%$, and $B = 0$.

toward the suction side and the exit angle deviates from the design angle, both a result of thickening boundary layers and the onset of separation.

To document the separation region, boundary-layer traverses were made using a hot-film probe at 68, 73, 75, 77, 84, and 92% axial chord for the case of $Re = 2.5 \times 10^4$ (Fig. 5). At 68% chord, the profile is highly unsteady in the region $y < 0.2$ cm, with instantaneous velocities (not shown) periodically dropping to near zero. Even with 4 s of averaging, the data do not all collapse cleanly onto the mean profile in the near-wall region. This indicates that the leading edge of the separation bubble is unsteady and periodically moves upstream of the 68% chord station. At the next station, 73% chord, the mean data is just beginning to indicate a thin separation zone. By the 75% station, the boundary layer is clearly separated and remains so through the three subsequent stations, 77, 84, and 92% chord, with velocities in the separated region falling below the calibrated range of the probe. Because a single hot-film probe was used, no flow direction information was available, and reverse flow can not be resolved. Separate smoke flow visualization confirmed that flow reversal was present inside the separation bubble at the 73% measurement station and that the recirculation zone inside the separation extended past the trailing edge of the blade.

At an inlet Reynolds number of 8.5×10^4, boundary-layer velocity data at similar axial stations indicated well-behaved laminar or

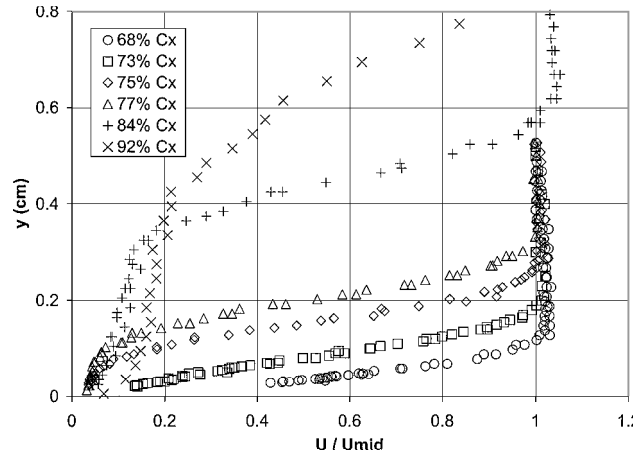

Fig. 5 Boundary-layer profiles of streamwise velocity normalized by midchannel velocity with no VGJ blowing ($B = 0$), $Re = 2.5 \times 10^4$, $T_u = 1\%$; profiles at six chordwise stations: 68, 73, 75, 77, 84, and 92% axial chord.

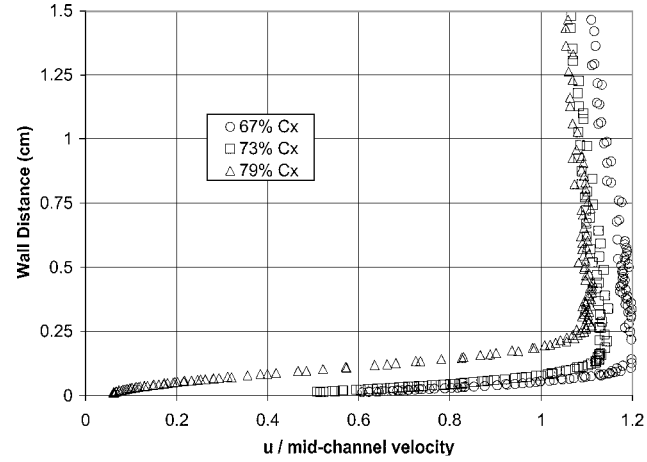

Fig. 6 Boundary-layer profiles of streamwise velocity normalized by midchannel velocity with no VGJ blowing ($B = 0$), $Re = 8.5 \times 10^4$, $T_u = 1\%$; profiles at three chordwise stations: 67, 73, and 79% axial chord.

transitional flow, at least up to the 79% chord position where the profile indicates an incipient separation (Fig. 6). This reduction in the separation zone with increasing Reynolds number is in agreement with the wake profiles shown in Fig. 4 and the surface-pressure measurements in Fig. 3.

Figure 7 shows a velocity power spectra taken with a hot wire just off of the blade wall, within the separation bubble, at 77% axial chord for a Reynolds number of 2.5×10^4. The peak at 100 Hz is the natural shedding frequency of the separation zone because it appears in spectra throughout the separation region and out into the wake and freestream, but does not appear in spectra in which the separation has been suppressed (Fig. 7).

Blowing at 63% Axial Chord

The effect of vortex-generator jet blowing on the turbine blade boundary-layer separation is dramatic. Figure 8 shows the local loss coefficient γ_{loc} profile for blade 5 for VGJ blowing ratios of 0, 1, 2, and 4, with injection at 63% axial chord. This injection location was chosen for detailed study because it sits in the middle of a rather broad region where VGJs are effective at suppressing the separation at $Re = 2.5 \times 10^4$ (see later discussion). The VGJs effectively eliminate the suction side separation zone, leaving a much narrower loss profile with a much reduced peak loss. The deviation of the peak loss from the projected inviscid trailing-edge extension line is due to the exit angle deviation caused by the thick blade boundary layer at a Reynolds number of 2.5×10^4. VGJ control of

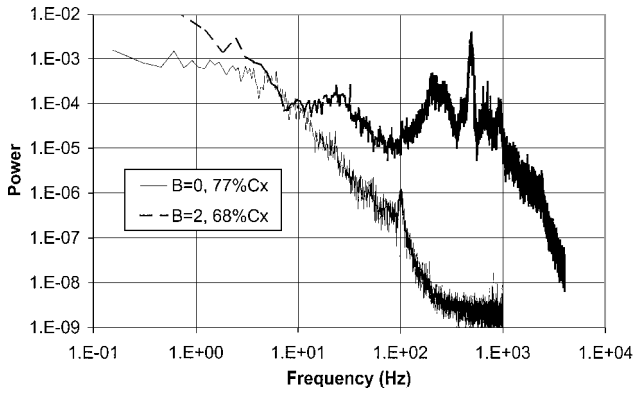

Fig. 7 Boundary-layer spectra for $Re = 2.5 \times 10^4$, 0.1 cm off surface; $B = 0$ at 77% C_x (separated flow); and $B = 2$ at 68% C_x (controlled flow).

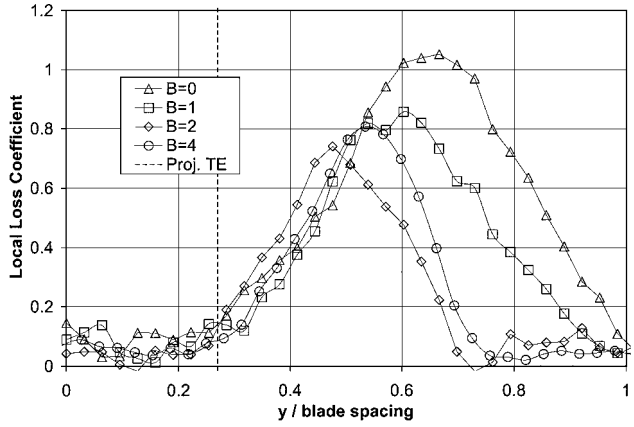

Fig. 8 Local pressure loss coefficient γ_{loc}; traverses across exit wakes at 0.62 C_x downstream from blade trailing, vertical dashed line is trailing-edge projection based on inviscid flow: $Re = 2.5 \times 10^4$, $T_u = 1\%$, and $B = 0$, 1, 2, and 4 at 63% C_x.

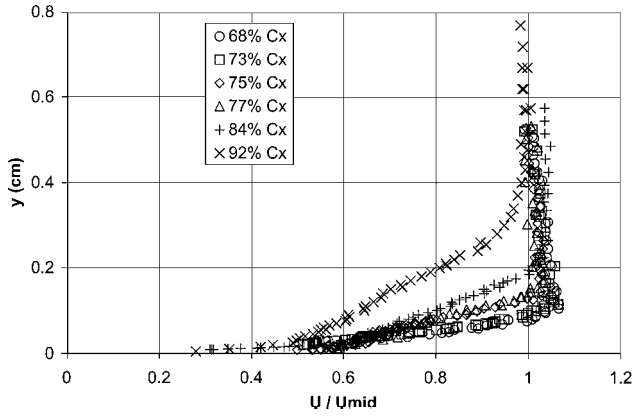

Fig. 9 Boundary-layer profiles of streamwise velocity, normalized by midchannel velocity; profiles at six chordwise stations: 68, 73, 75, 77, 84, and 92% axial chord, $Re = 2.5 \times 10^4$, $T_u = 1\%$, and $B = 2$ at 63% C_x.

the boundary-layer separation was corroborated by boundary-layer traverse data at the same six chordwise stations presented for the baseline blade. In Fig. 9, all of the measurement stations show a fully attached boundary layer, at least to the 92% chord position.

Figure 10 shows the spanwise variation of the boundary layers at the 68% (12d downstream of the VGJ injection) and 83% (59d downstream of the VGJ injection) chord locations, respectively. The three spanwise locations cover a single midspan pitch of the VGJ holes, with the first ($z = 0$ cm, midspan) and third ($z = 2$ cm) lined up with consecutive holes. The 68% profiles (open symbols) clearly show the impact of the blowing in the boundary layer close to the VGJs, with the midpitch ($z = 1$ cm) station profile significantly different than the other locations. By the 83% station (solid symbols) the VGJs have mixed out, and there is no longer any coherent spanwise variation.

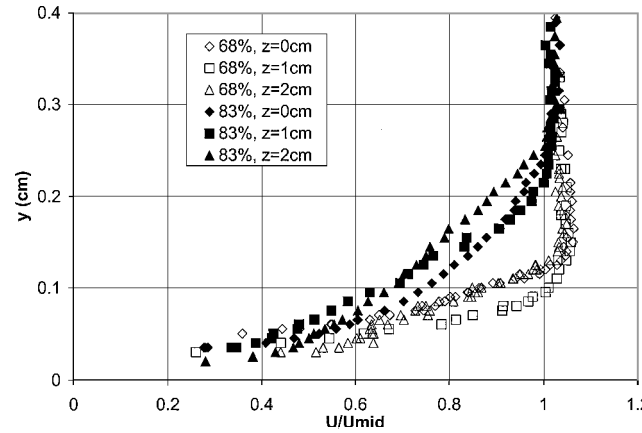

Fig. 10 Boundary-layer profiles at three spanwise stations, $Z = 0$ and $z = 2$ cm aligned with VGJ holes, $z = 1$ cm between VGJs; measurements at 68 and 83% C_x: $Re = 2.5 \times 10^4$, $T_u = 1\%$, and $B = 2$ at 63% C_x.

These data shed light on the fluid mechanism responsible for the separation control. The injected jets are at a skew of 90 deg relative to the freestream. As such, they possess negligible streamwise momentum and can not of themselves energize the boundary layer and eliminate separation. As noted in the water-tunnel experiments of Lin et al.,[6] varying the skew of VGJs from 0 to 90 deg has two notable effects on the generation of streamwise vortices in the flow. First, the two legs of the horseshoe vortex, which are of equal strength at a skew of 0 deg, become one dominant and one weak vortex at higher skew angles. Second, with adequate jet pitch (30–45 deg) and at high skew angles, the stronger vortex is forced down near the wall. The result is a single, strong vortex with great potential for mixing between the freestream and the boundary layer. The formation of this vortex, with its associated pumping of high-momentum fluid into the boundary layer, is a likely mechanism for separation control in the data presented here. In addition, the jets can also serve as boundary-layer trips. Boundary-layer instabilities generated by the flow around the VGJ injection sites can rapidly accelerate boundary-layer transition, contributing to separation prevention. Evidence of such instabilities is found in spectra taken just downstream of the injection site, at 68% chord (Fig. 7). The strong energy peak at 500 Hz corresponds to the Strouhal number of 0.2 shedding frequency of the freestream around the 1-mm-diam jets. This contributing mechanism of transition is only effective for low freestream turbulence cases. For the elevated turbulence cases (4%) the boundary layers are already transitional near the natural separation point, as will be discussed later. The primary mechanism remaining is freestream entrainment.

Figure 11 shows the pressure loss coefficient γ vs blowing ratio B for the 63% injection location. This plot, and the following loss coefficient plots, are actually composite data sets. Originally, two sets of data were obtained. One data set was loss coefficient vs blowing ratio for blowing only on the single ASC blade, with all of the other blades in the cascade untouched. The other data set was loss coefficient vs blowing ratio for blowing on the ASC blade while the other blades in the cascade were each tripped with an 0.5-mm-diam wire at 45% axial chord. The purpose of the trips was to simulate control on all of the blades of the cascade, though the trips are not as effective as the VGJs. The plots were formed by combining the loss coefficients from the untripped data for blowing ratios for which blowing was ineffective and the loss coefficients from the tripped data for blowing ratios for which the blowing was effective. This models the effect of blowing on all of the blades in the cascade for a range of blowing ratios that go from ineffective near $B = 0$ to effective at higher ratios. This approach was motivated by the observation that blowing applied to the ASC blade affected the flow on the adjacent blade 6.

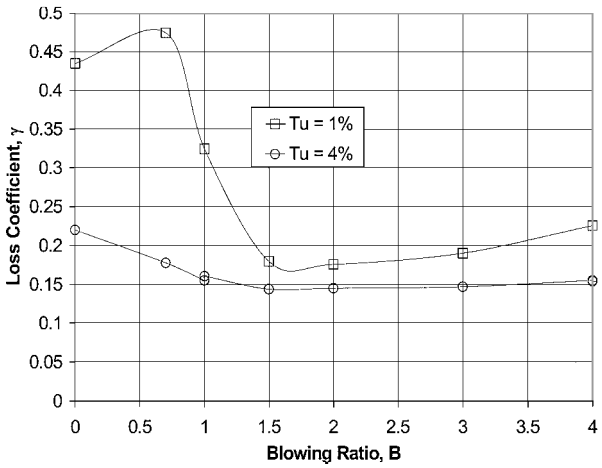

Fig. 11 Loss coefficient γ vs jet blowing ratio B for $Re = 2.5 \times 10^4$, $T_u = 1$ and 4%; injection at 63% C_x, composite data (see text).

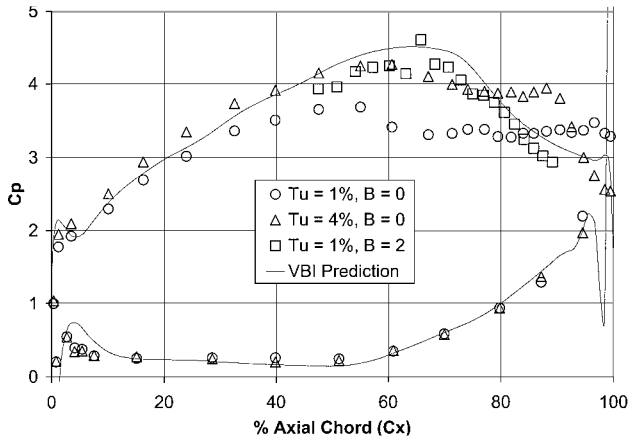

Fig. 12 Surface pressure coefficient vs axial chord for ASC blade: $Re = 2.5 \times 10^4$, $T_u = 1\%$, $B = 0$ (baseline, $L = 2.00$), $T_u = 1\%$, $B = 2$, plus trips at 45% C_x on adjacent blades ($L = 2.15$), $T_u = 4\%$, $B = 0$, and VBI prediction.

From Fig. 11, it can be seen that the minimum effective blowing ratio for this injection location and a turbulence level of 1% lies somewhere between 0.8 and 1. There is little change in the benefit of control between blowing ratios of 1 and 3, with an average wake loss reduction of 60% from the $B = 0$ case. Above a blowing ratio of 3, the losses begin to rise again. This is probably due to the strong jets blowing off the boundary-layer and creating a small premature separation. This could in turn both restart and transition the boundary layer, thereby suppressing the larger separation, but also adding losses.

Figure 12 shows the effect of blowing ($B = 2$) at the 63% axial chord location on the blade pressure coefficient with the non-ASC blades tripped. As is clearly shown, in addition to a dramatically reduced wake signature, the attached boundary layer also results in a higher pressure loading on the blade. This translates into an increase in the available work from a turbine rotor as measured by the blade loading parameter defined hereafter. This parameter represents the component of the integrated blade c_p distribution contributing to the direction of rotation (for a rotating stage):

$$L = \int_{\text{fullblade}} \left(\frac{P_{T,\text{in}} - P_{S,\text{loc}}}{P_{T,\text{in}}} \right) \frac{(\hat{e}_n \cdot \hat{e}_t)}{C_x} \, \mathrm{d}s \qquad (1)$$

This parameter is similar to the lift coefficient for external airfoils, which have significantly less camber than turbine airfoils. With VGJ control, the loading parameter L increased from a baseline value of 2 to 2.15 (approximately 7%).

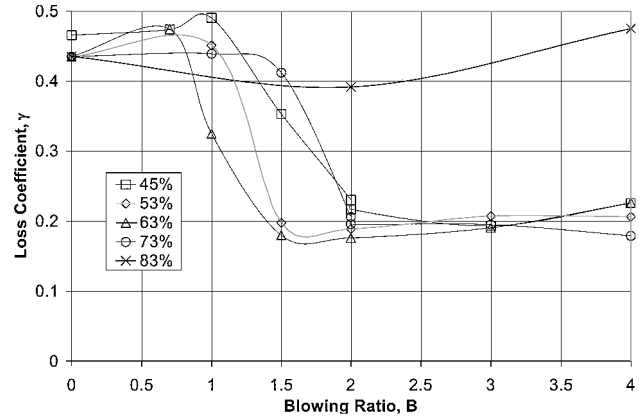

Fig. 13 Loss coefficient γ vs blowing ratio B for various injection locations: $Re = 2.5 \times 10^4$ and $T_u = 1\%$.

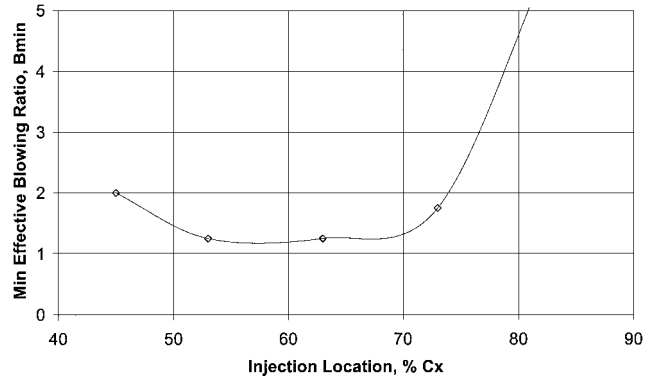

Fig. 14 Minimum effective blowing ratio $B_{\min}$ vs injection location: $Re = 2.5 \times 10^4$ and $T_u = 1\%$.

Effect of VGJ Location

The wide range of effective blowing ratios at the 63% injection location indicates that the exact location of the VGJ may not be a strong factor in determining the effectiveness of the separation control. Because the vortex strength decays exponentially with downstream distance,[4] there must, however, be practical limitations to the placement location. To study this, VGJ rows were implemented at four other chordwise locations on the ASC blade: well upstream of the separation point at 45 and 53% chord and downstream of the separation point at 73 and 83% chord. Each VGJ row was tested independently, with the other four rows sealed. Figure 13 shows plots of the loss coefficient vs jet blowing ratio for each of the five VGJ rows at an inlet Reynolds number of 2.5×10^4. The separation control provided by the VGJs was effective for all of the locations tested except the 83% chord location. This location is deep in the separation bubble, and so this result is not surprising. The VGJs did appear to become effective at $B > 4$ for the 83% location, but these data are not presented here. All of the other injection locations proved effective with only minor changes in the minimum required blowing ratio.

Figure 14 shows a plot of minimum effective blowing ratio vs VGJ injection location. A blowing ratio of $B = 2$ proved to be effective over nearly 30% of the chord of the blade. The implication of this is that this control technique should be effective even if the actual location of the separation is known only imprecisely.

Effect of Reynolds Number

As noted in the baseline data presentation, the subject blades show a dramatically reduced loss coefficient with increasing Reynolds number (Fig. 2). This is associated with a reduction in the size of the separation zone (Figs. 3 and 4). Accordingly, the effect of the application of VGJs at Reynolds numbers higher than 5×10^4 is not as striking. At a Reynolds number of 8.5×10^4, blowing at 63% chord produces a moderate (<10%) reduction in loss coefficient for

blowing ratios between 1 and 3. This is due to the suppression of the very small separation bubble that occurs at the rear of the blade at this Reynolds number (Fig. 3, circles). Above a blowing ratio of 3, there is a small increase in the loss coefficient over the unblown baseline, again likely due to the lift off of the boundary layer induced by the strong jets.

Effect of Elevated Freestream Turbulence

The insertion of the turbulence-generating grid significantly alters the blade boundary layer. The elevated freestream turbulence (4% just upstream of the cascade) accelerates boundary-layer transition on the suction surface, moderating the onset of separation as was seen in Fig. 2. Figure 12 shows the blade c_p profiles at a Reynolds number of 2.5×10^4 with and without the turbulence generator grid ($T_u = 1$ and 4%). The plateau associated with separation is reduced considerably from the low freestream turbulence case. Near-wall u' data at 67% C_x also clearly indicate a transitional boundary layer for 4% inlet turbulence, which would be more separation resistant. Figure 11 shows a plot of loss coefficient vs blowing ratio for the 4% freestream turbulence case. As expected, the benefits of separation control are not as striking for this case, for the simple reason that the separation losses are smaller to begin with. A 30% improvement in loss coefficient is achieved at a blowing ratio of about 1.5, again with a wide range of effective blowing ratios available. Measurements in an engine environment by Sharma[1] indicate that the freestream turbulence levels actually seen by the LPT are on the order of 10%. Although higher than the turbulence levels here, the effect of further increasing freestream turbulence is to cause a more rapid transition and reattachment in any separation that does occur. This effectively causes the separation-associated losses to increase more gradually as Reynolds number drops, as a result reducing the Reynolds number for which no reattachment (full separation) occurs (see Fig. 2). More detailed study into the effects of turbulence, particularly turbulence scales and the effects of bulk unsteadiness (upstream wakes), needs to be completed before definitive conclusions can be drawn for high-turbulence cases.

Conclusions

Active boundary-layer separation control has been successfully demonstrated on a low-pressure turbine blade using VGJs. The experiments were performed in a low-speed linear cascade using a typical high-performance blade shape with documented separation problems at low Reynolds numbers. The following conclusions are put forward based on the data presented:

1) VGJs drastically reduce suction surface boundary-layer separation at low Reynolds numbers. This is established for both low (<1%) and moderate (4%) levels of freestream turbulence. Higher turbulence levels need to be studied in more detail.

2) A minimum blowing ratio is required to reduce separation effectively. VGJ performance is essentially flat above this minimum blowing, with only a slight increase in losses at very high blowing ratios.

3) VGJs have proven to be effective at separation control over a wide range of injection locations with respect to the nominal separation point. This includes injection locations inside the separation bubble and as much as 25% chord upstream of the separation.

These results lead the authors to conclude that the application of VGJs for low Reynolds number separation control on LPT blades shows great promise.

Acknowledgments

This work was performed under partial sponsorship from the Air Force Office of Scientific Research, Thomas Beutner Contract Monitor. The authors are indebted to the Air Force Institute of Technology Machine Shop personnel (Russell Hastings, Jan LeValley, and Condie Inman) for the fine craftsmanship demonstrated in the construction of the wind tunnel used for this study. Also, this work would not have been possible without the technical expertise of U.S. Air Force Research Laboratory technician William Nilson. The efforts of James Lake are also acknowledged.

References

[1]Sharma, O., "Impact of Reynolds Number on LP Turbine Performance," *Proceedings of the 1997 Minnowbrook II Workshop on Boundary Layer Transition in Turbomachines*, NASA CP-1998-206958, 1998, pp. 65–69.

[2]Lin, J. C., Howard, F. G., Bushnell, D. M., and Selby, G. V., "Investigation of Several Passive and Active Methods of Turbulent Flow Separation Control," AIAA Paper 90-1598, 1990.

[3]Johnston, J. P., and Nishi, M., "Vortex-Generator Jets: Means for Flow Separation Control," *AIAA Journal*, Vol. 28, No. 6, 1990, pp. 989–994.

[4]Compton, D. A., and Johnston, J. P., "Streamwise Vortex Production by Pitched and Skewed Jets in a Turbulent Boundary-Layer," *AIAA Journal*, Vol. 30, No. 3, 1992, pp. 640–647.

[5]Henry, F. S., and Pearcey, H. H., "Numerical Model of Boundary-Layer Control Using Air-Jet Generated Vortices," *AIAA Journal*, Vol. 32, No. 12, 1994, pp. 2415–2425.

[6]Lin, J. C., Selby, G. V., and Howard, F. G., "Exploratory Study of Vortex-Generating Devices for Turbulent Flow Separation Control," AIAA Paper 91-0042, 1991.

[7]Rao, K. V., Delaney, R. A., and Topp, D. A., "Turbine Vane–Blade Interaction: Vol. 1, 2-D Euler/Navier–Stokes Aerodynamic and Grid Generation Developments," U.S. Air Force Research Lab., Rept. WL-TR-94-2073, Wright–Patterson AFB, OH, Jan. 1994.